Anomalous conductance quantization of a one-dimensional channel in monolayer WSe2

Adina Luican-Mayer (luican-mayer@uottawa.ca)
University of Ottawa https://orcid.org/0000-0001-9537-4600

Justin Boddison-Chouinard
University of Ottawa

Alex Bogan
National Research Council of Canada

Pedro Barrios
National Research Council of Canada

Jean Lapointe
National Research Council of Canada

Kenji Watanabe
National Institute for Materials Science https://orcid.org/0000-0003-3701-8119

Takashi Taniguchi
National Institute for Materials Science, Tsukuba, Ibaraki https://orcid.org/0000-0002-1467-3105

Jaroslaw Pawlowski
Wroclaw University od Science and Technology https://orcid.org/0000-0003-3638-3966

Daniel Miravet
University of Ottawa https://orcid.org/0000-0002-2908-4645

Maciej Bieniek
Wroc law University of Science and Technology

Pawel Hawrylak
University of Ottawa

Louis Gaudreau
National Research Council of Canada

Article

Keywords:

Posted Date: October 25th, 2022

DOI: https://doi.org/10.21203/rs.3.rs-2133454/v1

Anomalous conductance quantization of a one-dimensional channel in monolayer WSe_2

Justin Boddison-Chouinard,[1] Alex Bogan,[2] Pedro Barrios,[3] Jean Lapointe,[3] Kenji Watanabe,[4] Takashi Taniguchi,[5] Jarosław Pawłowski,[6] Daniel Miravet,[1] Maciej Bieniek,[7,6] Pawel Hawrylak,[1] Adina Luican-Mayer,[1,*] and Louis Gaudreau[2,†]

[1] *Department of Physics, University of Ottawa, Ottawa, Ontario, K1N 9A7*

[2] *Emerging Technologies Division, National Research Council of Canada, Ottawa, Ontario, K1A 0R6*

[3] *Advanced Electronics and Photonics, National Research Council of Canada, Ottawa, Ontario, K1A 0R6*

[4] *Research Center for Functional Materials, National Institute for Materials Science, 1-1 Namiki, Tsukuba 305-0044, Japan*

[5] *International Center for Materials Nanoarchitectonics, National Institute for Materials Science, 1-1 Namiki, Tsukuba 305-0044, Japan*

[6] *Department of Theoretical Physics, Wrocław University of Science and Technology, Wrocław, Poland*

[7] *Institute of Theoretical Physics, Wurzburg University, Wurzburg, Germany*

Among quantum devices based on 2D materials, gate-defined quantum confined 1D channels are much less explored, especially in the high mobility regime where many body interactions play an important role. We present results of measurements and theory of conductance quantization in a gate-defined one dimensional channel in a single layer of transition metal dichalcogenide material WSe_2. In the quasi-ballistic regime of our high mobility sample, we report conductance quantization steps in units of e^2/h for a wide range of carrier concentrations. Magnetic field measurements show that as the field is raised higher conductance plateaus move to accurate quantized values and then shift to lower conductance values while the e^2/h plateau remains locked. Based on microscopic atomistic tight-binding theory, we show that in this material, valley and spin degeneracies result in 2 e^2/h conductance steps for non-interacting holes, suggesting that symmetry breaking mechanisms such as valley polarization dominate the transport properties of such quantum structures.

INTRODUCTION

Realization of quantum devices based on two-dimensional (2D) materials has attracted significant interest in recent years [1, 2]; in particular, advances in fabrication techniques for devices based on transition metal dichalcogenides (TMDs) enabled the realisation of building blocks of quantum circuits such as gate-controlled quantum dots in monolayer and few layer MoS_2[3–5] and WSe_2[6, 7] as well as one-dimensional (1D) channels based on split gate technology[8–12]. 1D channels are of great interest in quantum information science because they have been established as valuable tools for non-invasive readout of semiconducting charge and spin qubits in GaAs[13], SiGe[14], graphene[15–18], bilayer graphene[19, 20] and WSe_2[21]. In 1D channels, the Landauer-Buttiker formalism explains the quantized conductance in units of $n\ e^2/h$, where n is the number of available transport channels, which depends on the degeneracies of the system; for example, 2-fold spin degeneracy for GaAs[22] and 4-fold spin and valley degeneracy for graphene[23]. Beyond this picture, much less is known about the mechanisms through which interaction effects can add complexity and play a role in transport anomalies [22]. Therefore, 1D channels based on high mobility 2D materials offer the possibility to access interaction regimes.

Here, we present results of investigation of the first 1D channel based on high mobility monolayer WSe_2, and find that the conductance is quantized in units of e^2/h. This is surprising since in monolayer TMDs, due to spin-valley locking, we expect conductance quantization for non-interacting holes in units of 2 e^2/h. Our results are in agreement with reports using few-layer MoS_2[8, 10], trilayer WSe_2[12] and monolayer MoS_2[9], but the origin of the e^2/h quantization remains unexplained. We attribute this broken valley and spin degeneracy to the formation of valley and spin polarised states of holes, which have been predicted for WS_2 [24, 25] and in laterally gated MoS_2 quantum dots [26, 27].

* luican-mayer@uottawa.ca
† louis.gaudreau@nrc-cnrc.gc.ca

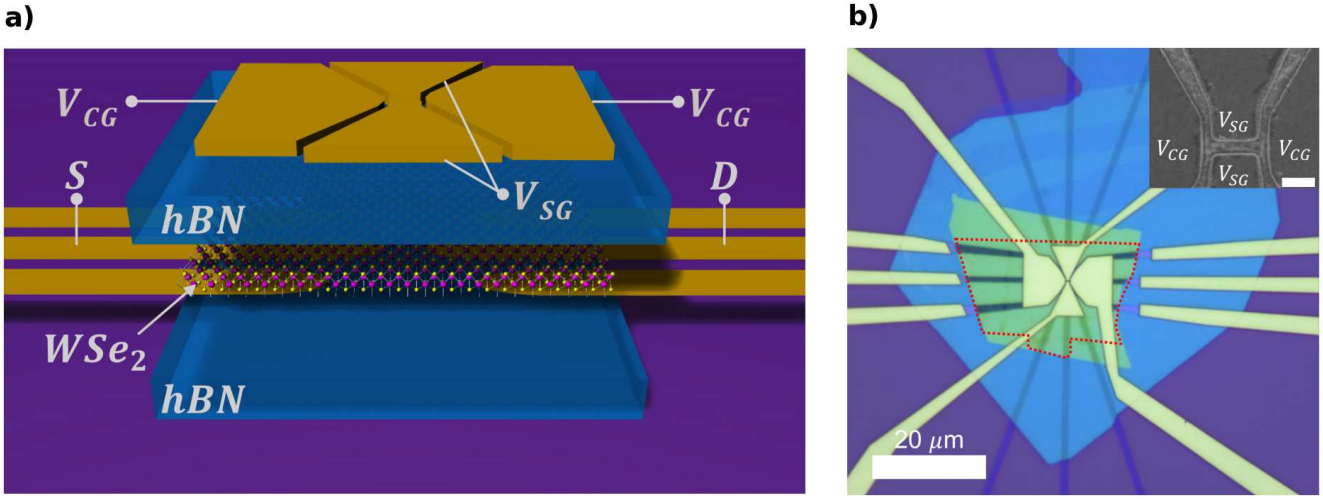

FIG. 1. (a) Schematic of the monolayer WSe_2 device structure. (b) Optical micrograph of the device used in this study. The WSe_2 monolayer flake is outlined in red for clarity. Inset: Scanning electron micrograph of the top gate structure (scalebar is 400 nm). The left and right gates are used to activate the contact region (V_{CG}). The top and bottom gates (V_{SG}) are used to form the 1D channel. The 1D channel is lithographically defined to have a width of 200 nm and a length of 600 nm.

Although there is already a substantial body of work explaining non-universal conductance quantization, a full understanding of the so called "0.7 anomaly" in quantum point contacts remains elusive and is assumed to be due to electron-electron interactions [28–37]. While the full theory of conductance in the presence of hole-hole interactions is in progress, here we show a complete single-particle model based on atomistic tight-binding theory for holes in a WSe_2 monolayer, confined in an electrostatically-defined 1D channel. It demonstrates that a channel potential does not break valley degeneracy and without hole-hole interactions conductance is expected to be quantized in units of 2 e^2/h. Hence the observed anomalous quantization in units of e^2/h can likely be explained in terms of broken symmetry valley-polarized ground state induced by interactions [24, 25, 38].

RESULTS

Device structure

Using standard dry transfer methods[39, 40], a van der Waals heterostructure consisting of a monolayer WSe_2 flake encapsulated between two hexagonal boron nitride (hBN) flakes was assembled on a p-doped silicon substrate with 285 nm of thermally grown silicon dioxide (SiO_2). The silicon substrate was utilized as a back gate to introduce carriers in the WSe_2 layer. Electron beam lithography was used to define electrical contacts [Cr (2 nm) / Pt (8 nm)][41], which contact the WSe_2 from the bottom, and to pattern a 4-component top gate. Two of the top gates, labelled as V_{CG} in Fig. 1a, cover the area where there is overlap between the WSe_2 flake and the electrical contacts, and are used to activate the electrical contacts. The two other top gates, labelled as V_{SG} in Figure 1a, were used to define the 1D channel in the WSe_2 with a lithographic width of 200 nm and length of 600 nm as confirmed by a scanning electron micrograph (Fig. 1b inset). Many important cleaning techniques were employed throughout the fabrication procedure and are detailed in the methods section. Figure 1b shows an optical micrograph of the completed device.

Electrical transport in a WSe_2 1D channel

We first demonstrate that we can create a conduction region with sufficiently low resistance to study quantized conductance. Figure 2a is a 4-point measurement of the device resistance R_{SD} as a function of the split gate voltage V_{SG} at a source-drain bias of 20 μV and constant back gate voltage $V_{BG} = -33\ V$. At low V_{SG}, when the voltages on the split gate are not sufficiently high to deplete the underlying WSe_2 regions from carriers, we measure a resistance of 480 Ω from which we are able to extract a contact resistance of 9.76 $k\Omega$ (see supplementary material section 1), a value that is comparable to others reported using more complex fabrication techniques[12, 42, 43]. As the voltage is increased on the split gates, we observe an increase in resistance indicating that a constriction has been formed and that holes are responsible for transport in the device.

The change in the conductance of the device in units of e^2/h as a function of the split gate voltage V_{SG} is shown in Figure 2b, from which we obtain a gate depletion value of $V_{SG} = 2.7\ V$. At this point, the 1D channel is formed, and

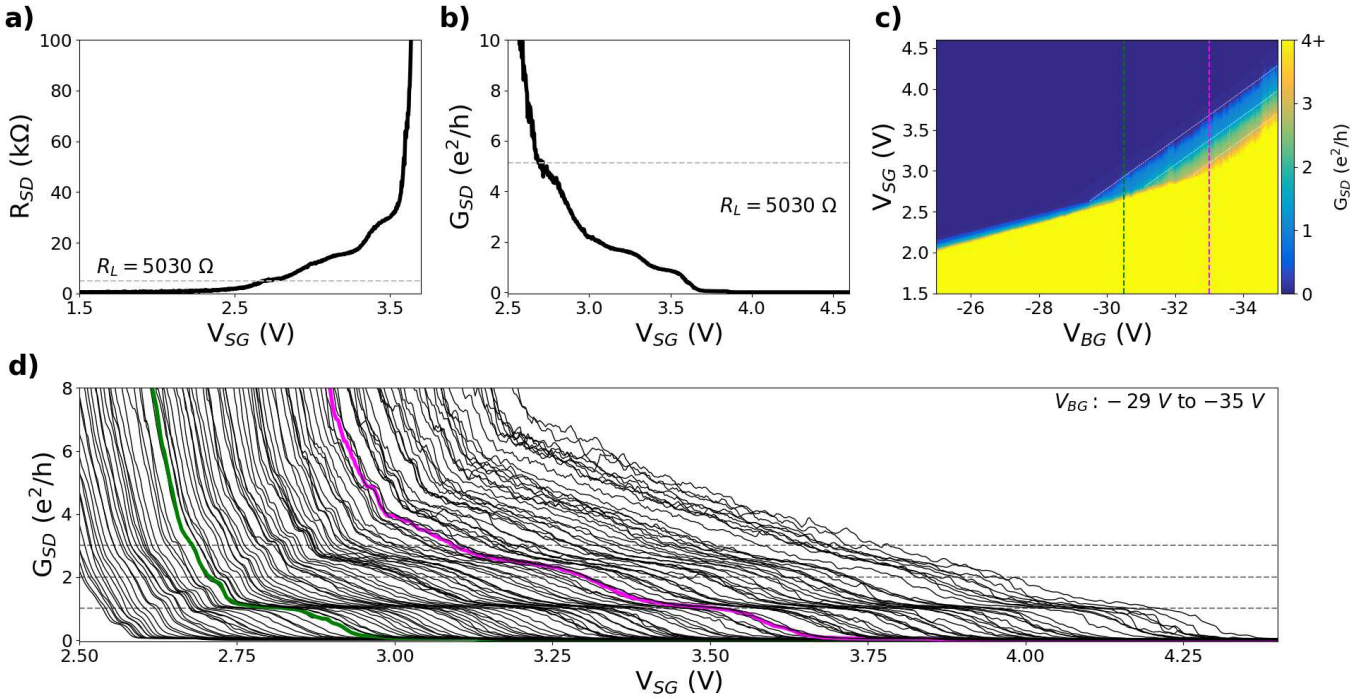

FIG. 2. (a) 4-point measurement of resistance vs. split gate voltage (V_{SG}) at $V_{BG} = -33$ V. The dashed line indicates the resistance where the channel is formed (at depletion). (b) Conductance in units of e^2/h vs. split gate voltage (V_{SG}) at $V_{BG} = -33$ V. The dashed line represents the conductance where the channel is formed (at depletion). (c) Color map of conductance as a function of split gate voltage V_{SG} and back gate voltage V_{BG}. A lead resistance (resistance at depletion) is subtracted. (d) Line cuts from (c) plotted in a "waterfall" style indicating a first step at e^2/h and a second step around 2 e^2/h. The left most trace is taken at $V_{BG} = -29$ V and the right most trace is taken at $V_{BG} = -35$ V. The green and magenta lines are highlighted by similarly colored dashed lines in (c) and correspond to back gate voltages of −30.5 V and −33 V respectively. These two curves feature the regimes where we observe the 1 e^2/h plateau (green), and the 1 e^2/h and 2 e^2/h plateaus (magenta).

the total measured resistance is 5030 Ω. When indicated, this back gate dependent series resistance (see supplementary material section 3) is subtracted from the raw data to obtain the conductance related only to the 1D channel[9]. In Figure 2b, quantized conductance steps close to e^2/h and 2 e^2/h can be observed for a fixed hole concentration of 1.82×10^{12} cm^{-2} (see supplementary material section 2). Tuning the concentration allows us to reach two different regimes, as demonstrated in Figure 2c. At higher hole concentrations, below $V_{BG} = -30\ V$, we see the appearance of the first conductance step at e^2/h. As the carrier concentration increases (V_{BG} decreases), the difference between the depletion and pinch-off values also increases and we observe the appearance of a second conductance step at a value of 2 e^2/h. These conductance steps are more clearly observed in a waterfall plot as shown in Figure 2d. The observation of quantized conductance through the 600 nm long channel along with the high measured field effect carrier mobility of $\mu_{FE} = 7900\ cm^2/Vs$[12, 41, 43, 44] (see supplementary material section 2), hints towards quasi-ballistic transport and demonstrates that a high quality monolayer WSe_2 sample has been achieved. At lower carrier concentrations, we observe the onset of a distinct transport regime that remains to be elucidated by further investigations (see supplementary material section 6).

Magnetic field dependence of the 1D channel

We further investigate the quantized conductance features by applying a magnetic field perpendicular to the plane of the two-dimensional material. Due to the large hole spin and valley g-factor which has been reported to be up to 12 in monolayer WSe_2[45], we explore the low magnetic field regime between −100 mT and 100 mT (Figure 3a) to eliminate any possible spin or valley polarisation occurring due to a small magnetic field offset at 0 T. The quantization remains constant at low field even at a high resolution of 4 mT. We therefore conclude that the measured lifting of spin and valley degeneracies at low fields is inherent to this particular system leading to a ground state where only one conducting channel is available. At higher fields, as depicted in Figure 3b, we observe that the first plateau remains constant between −5 T and 8 T with a very small correction around 0 T which we attribute to magnetoresistance effects in the leads. This magnetoresistance correction is more significant at higher conductance, but after 1.5 T we observe the second and third quantization plateaus aligning with the values of 2 e^2/h and 3 e^2/h. This data set

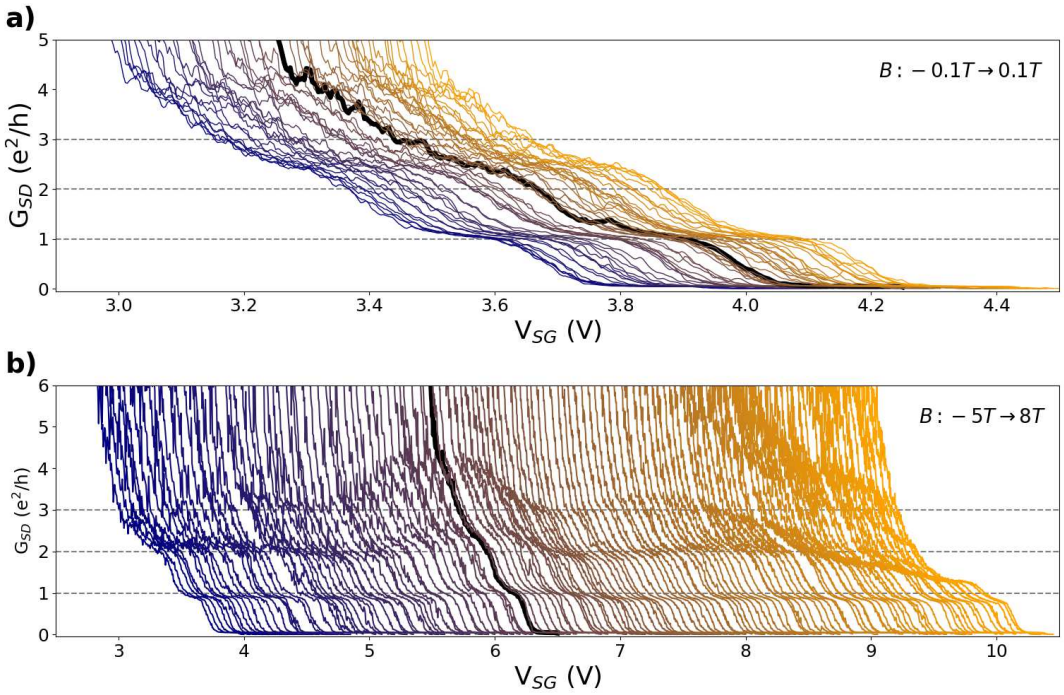

FIG. 3. (a) Dependence of the quantized conductance plateaus on a perpendicular low magnetic field ranging from −100 mT to 100 mT and a resolution of 4 mT. (b) Dependence of the quantized conductance plateaus on a perpendicular magnetic field ranging from –5 T to 8 T. In both panels, a horizontal offset is introduced between adjacent line traces for clarity. $V_{BG} = -33.2$ V for all runs with the corresponding lead resistance of $R_L = 5029\ \Omega$ subtracted.

demonstrates that each conductance channel up to the third one allows transport for only one quantum of conductance. We cannot determine, however, what is the ground state in terms of spin or valley. Additionally, at higher magnetic fields, we observe an evolution of the second and third plateaus in which they lower in conductance and seem to merge into the first plateau. No such change in conductance is observed for the first plateau. Measurements performed at 10 mK in a dilution refrigerator show the same behaviour (see supplementary material section 4).

Theory

In order to determine whether the anomalous quantization behaviour originates from the spin-valley locking mechanism in TMD's, we developed a single-particle model of a 1D channel. To calculate single-hole states, we use a tight-binding model for WSe_2 monolayer [26, 46–48] in a basis of three d-orbitals localized on tungsten atoms and three p-like orbitals describing Se_2 dimers (6 even orbitals in total).

A single-particle channel wavefunction for a hole state s satisfies the Schrödinger equation [47, 48]:

$$\left(H_{\text{bulk}} + |e|U^{\text{ch}}\right)|\Psi^s\rangle = E^s|\Psi^s\rangle, \tag{1}$$

where the channel is defined within the WSe_2 monolayer lattice and oriented along the x-axis of the elongated, rhombohedral computational box presented in Fig. 4(a). The 1D electronic confinement is determined by an applied external gate-defined potential U^{ch}. A hole is free to move in the channel direction, while movement in the perpendicular direction is constrained by a Gaussian-like potential along the y-axis:

$$U^{\text{ch}}(y) = U_0\left(1 - \exp\left(-\frac{y^2}{2\sigma_y^2}\right)\right), \tag{2}$$

parametrized in our calculations by potential depth $U_0 = 100$ mV, and width $\sigma_y = 5$ nm (see Fig. 4(a)). Note that at the center of the channel, where holes localize, the potential is zero and increases as we move away from the center.

We define the finite computational box in a form of a rhomboid of the WSe_2 lattice. We wrap the computational box on a torus, apply the periodic (Born–von Karman) boundary conditions, and obtain a set of allowed, discretized k-vectors over which we diagonalize the bulk Hamiltonian H_{bulk}. The valence band (VB) wavefunction for each

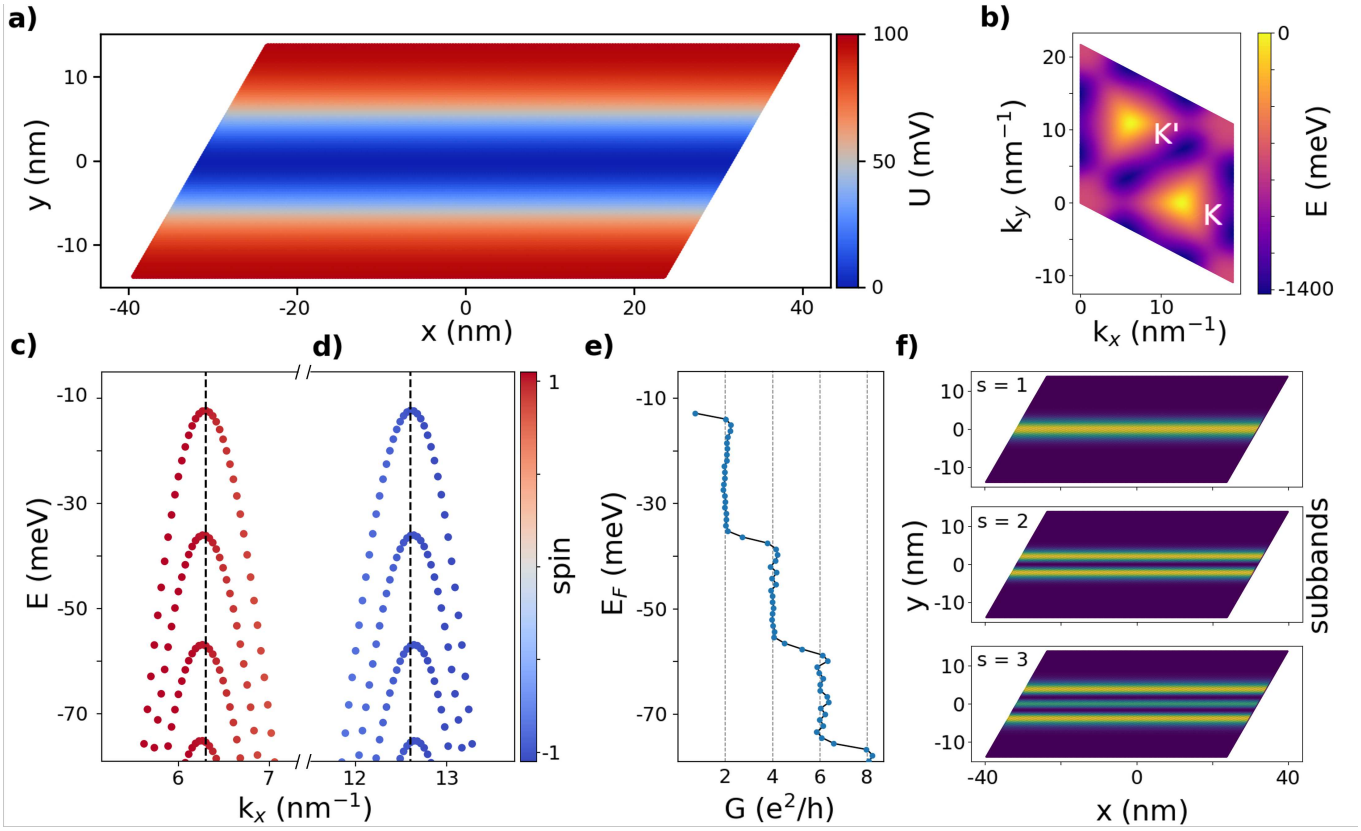

FIG. 4. (a) Computational rhombus representing WSe_2 monolayer with 1D gate-defined channel potential U^{ch} applied along the x-axis. (b) Valence band energy surface within the Brillouin zone with two maxima at K' and K points. (c,d) Single-particle states calculated within the tight-binding model for WSe_2 monolayer with applied 1D gate-defined channel potential U^{ch}. The hole eigenstates, characterized by their energy, wave vector k_x, and spin, form characteristic parabolic subbands located in (c) K' valley with spin-up (red dots), or (d) K valley with spin-down (blue dots). Subsequent subbands are used to calculate the channel conductance (d) via the Landauer formula. Resulting conductance curve has a characteristic stepped-like shape with subsequent plateaus at multiples of $2\ e^2/h$. Those states (numbered by s quantum number) are occupied by hole states with spatial densities (f) resembling harmonic oscillator modes.

allowed k-vector is a linear combination of Bloch functions on the W and Se_2 dimer sublattices l ($l = 1, \ldots, 6$):

$$|\psi^{\mathrm{VB}}_{k\sigma}\rangle = \sum_{l=1}^{6} A^{\mathrm{VB}}_{k\sigma l}\, |\psi_{k,l}\rangle \otimes |\chi_\sigma\rangle\,, \tag{3}$$

where $|\chi_\sigma\rangle$ is the spinor part of the wavefunction, and

$$|\psi_{k,l}\rangle = \frac{1}{\sqrt{N}} \sum_{R_l=1}^{N} e^{i\mathbf{k}\cdot\mathbf{R}_l} \varphi_l(\mathbf{r} - \mathbf{R}_l) \tag{4}$$

are Bloch functions built with atomic orbitals φ_l. N is the number of unit cells, while $\mathbf{R}_l$ defines the position of atomic orbitals in the computational rhomboid. By diagonalising the 6 by 6 Hamiltonian H_{bulk} at each allowed value of k we obtain the bulk energy bands $E^{\mathrm{VB}}_{k\sigma}$ and wavefunctions $A^{\mathrm{VB}}_{k\sigma l}$. The topmost valence band energy surface is shown in Fig. 4(b), where two non-equivalent maxima, K and K' valleys, are clearly visible.

In the next step, we expand the channel wavefunction in terms of the lowest energy valence band states given by Eq. 3:

$$|\Psi^s_\sigma\rangle = \sum_k B^{\mathrm{VB},s}_{k\sigma}\, |\psi^{\mathrm{VB}}_{k\sigma}\rangle\,. \tag{5}$$

Finally, we solve the Schrödinger equation (1) with the potential term U^{ch} by converting it to an integral equation for the coefficients $B^{\mathrm{VB},s}_{k\sigma}$, and obtain the single-hole eigenstates confined within the channel,

$$E^{\mathrm{VB}}_{q\sigma} B^{\mathrm{VB},s}_{q\sigma} + \sum_k B^{\mathrm{VB},s}_{k\sigma} \sum_l \left(A^{\mathrm{VB}}_{q\sigma l}\right)^* A^{\mathrm{VB}}_{k\sigma l}\, U^{\mathrm{ch}}_l(q,k) = E^s_\sigma B^{\mathrm{VB},s}_{q\sigma}, \tag{6}$$

where $U^{\mathrm{ch}}_l(q,k) = \frac{1}{N}\sum_{R_l=1}^{N} U^{\mathrm{ch}}(\mathbf{R}_l) e^{i(\mathbf{k}-\mathbf{q})\cdot\mathbf{R}_l}$ is the Fourier transform of the channel confinement on each sublattice l. The structural and the tight-binding Slater-Koster parameters in the calculations are directly listed in the supplementary material, Section 7.

The channel states of energy E^s_σ are characterized by subband index s, by the spin σ, and also by the valley K or K' determined by the expectation value of the wave vector $\langle k_x\rangle \equiv k_x$ in the channel direction. They belong to two different valleys: K' with spin-up – Fig. 4 (c), and K with spin-down – Fig. 4 (d), creating degenerate spin-valley locked states. Characteristic parabolic subbands are formed due to the lateral quantization within the channel represented by different values of s quantum number.

We note that the VB maximum (for the free hole Hamiltonian H_{bulk}) is shifted to zero and the highest energy state (ground state for holes in the channel) is located below, at -12 meV. The second spin-valley pair (not presented) is split-off by 0.5 eV below on the energy scale by the strong intrinsic spin-orbit coupling present in this material.

After calculating the single-particle eigenstates of the Hamiltonian H, we are ready to numerically estimate the conductance through the 1D channel. For each subband s, we calculate the density of states within the given subband $\frac{dN_s}{dE}$, and then estimate the particle velocity as $v_s(E) = \frac{1}{\hbar}\frac{\partial E_s}{\partial k_x}$. The conductance, which combines contributions from states from different occupied subbands s filled up to the Fermi energy, is calculated using the 2-terminal Landauer formula [49]:

$$G(E_F) = \frac{e^2}{E_F} \sum_s \int_0^{E_F} dE \frac{1}{2} \frac{dN_s}{dE} v_s(E). \tag{7}$$

The factor 1/2 is due to the fact that we take only states with $k_x > K_x$ (or $k_x > K'_x$ for the second valley), i.e., active under the given source-drain bias. In the above formula we assume that no backscattering occurs. The calculated conductance is presented in Fig. 4(e). It has the conductance plateaus at multiples of 2 e^2/h. The corresponding charge densities for each subband are plotted in Fig. 4(f). The final result shows that a microscopic theory of a 1D channel predicts conductance steps in units of 2 e^2/h. Hence, we see that the measured e^2/h conductance quantization cannot be explained in the single-particle picture.

A possible explanation for the e^2/h conductance quantization can be obtained in terms of a broken symmetry valley-polarized ground state [24, 25, 38]. A valley polarized state is expected to be the ground state of a 2D hole gas in a single layer of WSe_2 for sufficiently strong interaction strength and hole density (in analogy to WS_2 [25]). The breaking of valley degeneracy naturally lifts the degeneracy of bands in the mean field picture. Therefore, conductance plateaus in conductance quantization are expected to be half of the degenerate system, giving e^2/h instead of 2 e^2/h steps as a function of Fermi energy. This might explain the e^2/h plateau for a large range of hole densities, as shown in Fig. 2(d).

CONCLUSION

In summary, we have fabricated high quality monolayer WSe_2 devices where an electrostatically confined 1D hole transport channel is formed. At low temperature, hole quasi-ballistic transport is observed, revealing an unexpected conductance quantization in steps of e^2/h instead of 2 e^2/h taking into account the electronic effects from the band structure of TMDs such as spin-valley locking. We have compared the experimental results to a single particle atomistic tight-binding model for holes in WSe_2 and demonstrated that a 1D confining potential does not reproduce the measured conductance quantization in units of e^2/h. Recent experiments[24] and theory[26] suggest the existence of a valley polarised state of the hole gas in TMDs. Such a state would explain the measured plateau at e^2/h. A theoretical model which includes hole-hole correlations is therefore necessary to explain quantum transport in 2D TMDs. These results show that the electronic properties of monolayer TMDs are still insufficiently understood and require further research to elucidate.

METHODS

Device fabrication

The device was assembled on a p-doped silicon substrate with 285 nm of thermally grown silicon dioxide (SiO_2). Using standard dry transfer methods[39, 40], a flake of hexagonal boron nitride (hBN) (26 nm) was picked-up with a polypropylene carbonate (PPC) coated polydimethylsiloxane (PDMS) stamp and transferred onto lithographically patterned local gates. Electrical contacts [Cr (2 nm) / Pt (8 nm)][41] were subsequently patterned on top of the hBN. To remove any contaminants on the surface of the hBN and the electrical contacts, the sample was thermally annealed in a vacuum furnace (10^{-7} Torr) at 300 °C for 30 minutes and further cleaned mechanically using an atomic force microscope tip (AFM) in contact mode[7, 21, 50, 51]. A second polymer stamp was used to subsequently pick-up an hBN flake (34 nm) then a monolayer WSe_2 flake. To ensure proper contact to the electrical contacts, the stack of flakes and stamp were placed in an AFM such that the surface of the WSe_2 flake was exposed where it was then mechanically cleaned using an AFM tip. The hBN/WSe_2 stack was then dropped off onto the patterned contacts. At this stage, the device was thermally annealed in a vacuum furnace following the same recipe as before. A final lithographic step was performed to pattern the top gates which include the 2 contact top gates (V_{CG}) and the split gates (V_{SG}).

Tight-binding Parameters

In the tight-binding atomistic calculations we chose the following structural parameters: $d_{\|} = 1.9188$ Å (W-Se_2 dimer center distance), $d_{\perp} = 1.6792$ Å (Se atom distance from $z = 0$ plane). The tight-binding Slater-Koster parameters are given by (all in eV): $E_d = -0.4330$, $E_{p0} = -3.8219$, $E_{p\pm1} = -2.3760$, $V_{dp\sigma} = -1.58193$, $V_{dp\pi} = 1.17505$, $V_{dd\sigma} = -0.90501$, $V_{dd\pi} = 1.0823$, $V_{dd\delta} = -0.1056$, $V_{pp\sigma} = 0.52091$, $V_{pp\pi} = -0.16775$, together with characterising intrinsic spin-orbit couplings: $\lambda_W = 0.275$, $\lambda_{Se_2} = 0.08$. We note that these parameters are chosen to reproduce ab initio electronic band structure of two spinfull valence bands.

DATA AVAILABILITY

The data that support the findings of this study are available from the corresponding author upon reasonable request.

[1] X. Liu and M. C. Hersam, Nature Reviews Materials **4**, 669 (2019).
[2] A. Alfieri, S. B. Anantharaman, H. Zhang, and D. Jariwala, Advanced Materials , 2109621 (2022), https://onlinelibrary.wiley.com/doi/pdf/10.1002/adma.202109621.
[3] Z.-Z. Zhang, X.-X. Song, G. Luo, G.-W. Deng, V. Mosallanejad, T. Taniguchi, K. Watanabe, H.-O. Li, G. Cao, G.-C. Guo, F. Nori, and G.-P. Guo, Science Advances **3**, e1701699 (2017), https://www.science.org/doi/pdf/10.1126/sciadv.1701699.
[4] R. Pisoni, Z. Lei, P. Back, M. Eich, H. Overweg, Y. Lee, K. Watanabe, T. Taniguchi, T. Ihn, and K. Ensslin, Applied Physics Letters **112**, 123101 (2018), https://doi.org/10.1063/1.5021113.
[5] K. Wang, K. De Greve, L. A. Jauregui, A. Sushko, A. High, Y. Zhou, G. Scuri, T. Taniguchi, K. Watanabe, M. D. Lukin, H. Park, and P. Kim, Nature Nanotechnology **13**, 128 (2018).
[6] S. Davari, J. Stacy, A. Mercado, J. Tull, R. Basnet, K. Pandey, K. Watanabe, T. Taniguchi, J. Hu, and H. Churchill, Phys. Rev. Applied **13**, 054058 (2020).
[7] J. Boddison-Chouinard, A. Bogan, N. Fong, K. Watanabe, T. Taniguchi, S. Studenikin, A. Sachrajda, M. Korkusinski, A. Altintas, M. Bieniek, P. Hawrylak, A. Luican-Mayer, and L. Gaudreau, Applied Physics Letters **119**, 133104 (2021), https://doi.org/10.1063/5.0062838.
[8] R. Pisoni, Y. Lee, H. Overweg, M. Eich, P. Simonet, K. Watanabe, T. Taniguchi, R. Gorbachev, T. Ihn, and K. Ensslin, *Nano Letters*, Nano Letters **17**, 5008 (2017).
[9] K. Marinov, A. Avsar, K. Watanabe, T. Taniguchi, and A. Kis, Nature Communications **8**, 10.1038/s41467-017-02047-5 (2017).
[10] A. Epping, L. Banszerus, J. Güttinger, L. Krückeberg, K. Watanabe, T. Taniguchi, F. Hassler, B. Beschoten, and C. Stampfer, Journal of Physics: Condensed Matter **30**, 205001 (2018).
[11] C. S. Lau, J. Y. Chee, D. Thian, H. Kawai, J. Deng, S. L. Wong, Z. E. Ooi, Y.-F. Lim, and K. E. J. Goh, Scientific Reports **9**, 10.1038/s41598-019-45392-9 (2019).
[12] K. Sakanashi, P. Krüger, K. Watanabe, T. Taniguchi, G.-H. Kim, D. K. Ferry, J. P. Bird, and N. Aoki, Nano Lett. **21**, 7534 (2021).

[13] M. Field, C. G. Smith, M. Pepper, D. A. Ritchie, J. E. F. Frost, G. A. C. Jones, and D. G. Hasko, Phys. Rev. Lett **70**, 1311 (1993).
[14] C. B. Simmons, M. Thalakulam, N. Shaji, L. J. Klein, H. Qin, R. H. Blick, D. E. Savage, M. G. Lagally, S. N. Coppersmith, and M. A. Eriksson, Applied Physics Letters **91**, 213103 (2007), https://doi.org/10.1063/1.2816331.
[15] J. Güttinger, C. Stampfer, S. Hellmüller, F. Molitor, T. Ihn, and K. Ensslin, Appl. Phys. Lett. **93**, 212102 (2008).
[16] L. Wang, G. Cao, T. Tu, H.-O. Li, C. Zhou, Z. S. X.-J. Hao, G.-C. Guo, H.-W. Jiang, and G.-P. Guo, Appl. Phys. Lett. **97**, 262113 (2010).
[17] J. Güttinger, J. Seif, C. Stampfer, A. Capelli, K. Ensslin, and T. Ihn, Phys. Rev. B **83**, 165445 (2011).
[18] C. Volk, C. Neumann, S. Fringes, S. Engels, F. Haupt, A. Müller, and C. Stampfer, Nat. Commun. **4** (2013).
[19] S. Fringes, C. Volk, C. Norda, B. Terrés, J. Dauber, S. Engels, S. Trellenkamp, and C. Stampfer, Phys. Status Solidi B **248**, 2684 (2011).
[20] A. Kurzmann, H. Overweg, M. Eich, A. Pally, P. Rickhaus, R. Pisoni, K. Watanabe, T. Taniguchi, T. Ihn, and K. Ensslin, Nano Lett. **19**, 5216 (2019).
[21] J. Boddison-Chouinard, A. Bogan, N. Fong, P. Barrios, J. Lapointe, K. Watanabe, T. Taniguchi, A. Luican-Mayer, and L. Gaudreau, arXiv 10.48550/arXiv.2203.11871 (2022).
[22] K. J. Thomas, J. T. Nicholls, M. Y. Simmons, M. Pepper, D. R. Mace, and D. A. Ritchie, Phys. Rev. Lett. **77**, 135 (1996).
[23] H. Overweg, H. Eggimann, X. Cheng, S. Slizovskiy, M. Eich, R. Pisoni, Y. Lee, P. Rickhaus, K. Watanabe, T. Taniguchi, V. Fal'ko, T. Ihn, and K. Ensslin, Nano Lett. **18**, 553 (2017).
[24] T. Scrace, Y. Tsai, B. Barman, L. Schweidenback, A. Petrou, G. Kioseoglou, I. Ozfidan, M. Korkusiński, and P. Hawrylak, Nat. Nano. **10**, 603 (2015).
[25] J. a. E. H. Braz, B. Amorim, and E. V. Castro, Phys. Rev. B **98**, 161406 (2018).
[26] L. Szulakowska, M. Cygorek, M. Bieniek, and P. Hawrylak, Phys. Rev. B **102**, 245410 (2020).
[27] J. Pawłowski, M. Bieniek, and T. Woźniak, Phys. Rev. Applied **15**, 054025 (2021).
[28] K. J. Thomas, J. T. Nicholls, M. Y. Simmons, M. Pepper, D. R. Mace, and D. A. Ritchie, Phys. Rev. Lett. **77**, 135 (1996).
[29] S. M. Cronenwett, H. J. Lynch, D. Goldhaber-Gordon, L. P. Kouwenhoven, C. M. Marcus, K. Hirose, N. S. Wingreen, and V. Umansky, Phys. Rev. Lett. **88**, 226805 (2002).
[30] Y. Meir, K. Hirose, and N. S. Wingreen, Phys. Rev. Lett. **89**, 196802 (2002).
[31] T. Rejec and Y. Meir, Nature **442**, 900 (2006).
[32] K. A. Matveev, Phys. Rev. Lett. **92**, 106801 (2004).
[33] K. A. Matveev, Phys. Rev. B **70**, 245319 (2004).
[34] A. D. Güçlü, C. J. Umrigar, H. Jiang, and H. U. Baranger, Phys. Rev. B **80**, 201302 (2009).
[35] E. Welander, I. I. Yakimenko, and K.-F. Berggren, Phys. Rev. B **82**, 073307 (2010).
[36] A. C. Mehta, C. J. Umrigar, J. S. Meyer, and H. U. Baranger, Phys. Rev. Lett. **110**, 246802 (2013).
[37] A. P. Micolich, Journal of Physics: Condensed Matter **23**, 443201 (2011).
[38] M. Van der Donck and F. M. Peeters, Phys. Rev. B **98**, 115432 (2018).
[39] L. Wang, I. Meric, P. Y. Huang, Q. Gao, Y. Gao, H. Tran, T. Taniguchi, K. Watanabe, L. M. Campos, D. A. Muller, J. Guo, P. Kim, J. Hone, K. L. Shepard, and C. R. Dean, Science **342**, 614 (2013), https://www.science.org/doi/pdf/10.1126/science.1244358.
[40] J. Boddison-Chouinard, R. Plumadore, and A. Luican-Mayer, Journal of visualized experiments : JoVE (2019).
[41] H. C. P. Movva, A. Rai, S. Kang, K. Kim, B. Fallahazad, T. Taniguchi, K. Watanabe, E. Tutuc, and S. K. Banerjee, *ACS Nano*, ACS Nano **9**, 10402 (2015).
[42] E. J. Telford, A. Benyamini, D. Rhodes, D. Wang, Y. Jung, A. Zangiabadi, K. Watanabe, T. Taniguchi, S. Jia, K. Barmak, A. N. Pasupathy, C. R. Dean, and J. Hone, Nano Lett. **18**, 1416 (2018).
[43] Y. Jung, M. S. Choi, A. Nipane, A. Borah, B. Kim, A. Zangiabadi, T. Taniguchi, K. Watanabe, W. J. Yoo, J. Hone, and J. T. Teherani, Nature Electronics **2**, 187 (2019).
[44] H.-J. Chuang, X. Tan, N. J. Ghimire, M. M. Perera, B. Chamlagain, M. M.-C. Cheng, J. Yan, D. Mandrus, D. Tománek, and Z. Zhou, Nano Letters **14**, 3594 (2014).
[45] M. V. Gustafsson, M. Yankowitz, C. Forsythe, D. Rhodes, K. Watanabe, T. Taniguchi, J. Hone, X. Zhu, and C. R. Dean, Nature Materials **17**, 411 (2018).
[46] M. Bieniek, M. Korkusiński, L. Szulakowska, P. Potasz, I. Ozfidan, and P. Hawrylak, Phys. Rev. B **97**, 085153 (2018).
[47] M. Bieniek, L. Szulakowska, and P. Hawrylak, Phys. Rev. B **101**, 035401 (2020).
[48] A. Altıntaş, M. Bieniek, A. Dusko, M. Korkusiński, J. Pawłowski, and P. Hawrylak, Phys. Rev. B **104**, 195412 (2021).
[49] L. P. Kouwenhoven, G. Schön, and L. L. Sohn, Introduction to mesoscopic electron transport, in *Mesoscopic Electron Transport*, edited by L. L. Sohn, L. P. Kouwenhoven, and G. Schön (Springer Netherlands, Dordrecht, 1997) pp. 1–44.
[50] A. M. Goossens, V. E. Calado, A. Barreiro, K. Watanabe, T. Taniguchi, and L. M. K. Vandersypen, Applied Physics Letters **100**, https://doi.org/10.1063/1.3685504 (2012).
[51] M. R. Rosenberger, H.-J. Chuang, K. M. McCreary, A. T. Hanbicki, S. V. Sivaram, and B. T. Jonker, ACS Applied Materials & Interfaces **10**, https://doi.org/10.1021/acsami.8b01224 (2018).

ACKNOWLEDGMENTS

We would like to thank Dr. Andrew Sachrajda for his fruitful discussions. This work was supported by the High Throughput and Secure Networks Challenge Program and the Quantum Sensors Challenge Program at the National Research Council of Canada. This research was supported by NSERC QC2DM Strategic Grant No. STPG-521420, NSERC Discovery Grant No. RGPIN- 2019-05714, and University of Ottawa Research Chair in Quantum Theory of Quantum Materials, Nanostructures, and Devices. J.P. acknowledges support from National Science Centre, Poland, under grant no. 2021/43/D/ST3/01989. M.B. acknowledges financial support from the Polish National Agency for Academic Exchange (NAWA), Poland, grant PPI/APM/2019/1/00085/U/00001. This research was enabled in part by support provided by the Digital Research Alliance of Canada (alliancecan.ca). This research was supported in part by PL-Grid Infrastructure.

AUTHOR CONTRIBUTIONS

J.B.-C., A.B., and L.G. designed the device architecture. J.B.-C., P.B., and J.L. fabricated the top gate structure while J.B-C. fabricated the remainder of the device with inputs from A.L.-M. and L.G.. J.B.-C performed the experimental measurements and the data analysis with consultations from A.B., A.L.-M., and L.G.. Theoretical models and calculations were completed by J.P., D.M., M.B., and P.H.. K.W. and T.T. grew the hexagonal boron nitride crystals. All authors participated in the writing of the manuscript.

COMPETING INTERESTS

The authors declare no competing financial or non-financial interests.

Supplementary Files

This is a list of supplementary files associated with this preprint. Click to download.

- ConductancequantizationWsE2Supplementary.pdf